AMERICAN METEOROLOGICAL SOCIETY

Journal of Climate

EARLY ONLINE RELEASE

The DOI for this manuscript is doi: 10.1175/JCLI-D-14-00065.1

The final published version of this manuscript will replace the preliminary version at the above DOI once it is available.

If you would like to cite this EOR in a separate work, please use the following full citation:

Scoccimarro, E., S. Gualdi, G. Villarini, G. Vecchi, M. Zhao, K. Walsh, and A. Navarra, 2014: Intense precipitation events associated with landfalling tropical cyclones in response to a warmer climate and increased CO2. J. Climate. doi:10.1175/JCLI-D-14-00065.1, in press.

Intense precipitation events associated with landfalling tropical cyclones in response to a warmer climate and increased CO_2

Enrico Scoccimarro[1,2]*
Silvio Gualdi[1,2]
Gabriele Villarini[3]
Gabriel A. Vecchi[4]
Ming Zhao[4]
Kevin Walsh[5]
Antonio Navarra[1,2]

[1]Istituto Nazionale di Geofisica e Vulcanologia (INGV), Bologna, Italy

[2]Centro Euro-Mediterraneo sui Cambiamenti Climatici (CMCC), Bologna, Italy

[3]IIHR-Hydroscience & Engineering, The University of Iowa, Iowa City, Iowa

[4]Geophysical Fluid Dynamics Laboratory (GFDL), Princeton, New Jersey

[5]School of Earth Sciences, University of Melbourne, Melbourne, Australia

Manuscript submitted to Journal of Climate 17 January 2013

revised March 2014

Corresponding author address:

-Enrico Scoccimarro, Centro Euro-Mediterraneo sui Cambiamenti Climatici (CMCC), V.le A.Moro 44, 40127 Bologna, Italy. E-mail: enrico.scoccimarro@bo.ingv.it

Abstract:

In this work the authors investigate possible changes in the intensity of rainfall events associated with tropical cyclones (TCs) under idealized forcing scenarios, including a uniformly warmer climate, with a special focus on landfalling storms. A new set of experiments designed within the U.S. CLIVAR Hurricane Working Group allows disentangling the relative role of changes in atmospheric carbon dioxide from that played by sea surface temperature (SST) in changing the amount of precipitation associated with TCs in a warmer world. Compared to the present day simulation, we found an increase in TC precipitation under the scenarios involving SST increases. On the other hand, in a CO_2 doubling-only scenario, the changes in TC rainfall are small and we found that, on average, TC rainfall tends to decrease compared to the present day climate. The results of this study highlight the contribution of landfalling TCs to the projected increase in the precipitation changes affecting the tropical coastal regions.

1. Introduction

Heavy precipitation and flooding associated with tropical cyclones (TCs) are responsible for a large number of fatalities and economic damage worldwide (e.g., Rappaport 2000; Pielke et al. 2008; Mendelsohn et al. 2012; Peduzzi et al. 2012). Due in part to the societal and economic relevance of this hazard, studies have focussed on the potential changes in heavy rainfall associated with TCs in a warmer climate (Gualdi et al. 2008, Knutson and Tuleya 2004; Hasegawa and Emori, 2005; Knutson et al. 2013). Despite the overall agreement about the tendency of TC-rainfall to increase with greenhouse warming, the uncertainty of the projected changes is large, ranging from +3% to +37% (Knutson and Tuleya 2004, Knutson et al. 2010, 2013).

Models project a well known increase to rainfall over land, both in terms of average and extremes (e.g., Liu et al. 2009, Chou et al. 2009) and a large spatial variability is associated with changes in projected rainfall amount (Trenberth et al. 2011, Scoccimarro et al. 2013). The goal of this study is to quantify the contribution of landfalling TCs to rainfall at different latitudes, as well as its dependence on different idealized climate change scenarios.

TCs can deliver large amounts of precipitation in a relatively short time, and tropical cyclone precipitation (TCP) represents a significant portion of total summer precipitation along the tropical coastal regions (Jiang et al. 2010). For instance Larson et al. (2005) found that TCP contributes up to 20% of the total precipitation over the coast of Mexico. Individual storms can, however, account for more than 90% of the summer rainfall experienced in some regions, such as southern California (Corbosiero et al. 2009) and Australia (Dare et al. 2012), representing a significant water management challenge.

The investigation of TCP response to different idealized global warming scenarios is made possible by the availability of a set of high resolution General Circulation Models (GCMs) and simulations performed following common protocols, within the US-CLIVAR Hurricane Working

Group (http://www.usclivar.org/working-groups/hurricane). In our analyses, we will first assess whether these GCMs are able to reproduce TC rainfall contribution to the total rainfall at the global scale, with particular emphasis on the coastal regions. After the model evaluation, we will examine the changes in TCP for three idealized experiments, doubling CO_2, increasing the global sea surface temperature (SST) by 2 K, and a combination of the two. These idealized experiments are not based on projected emission scenarios, but designed to disentangle the role of changes in atmospheric carbon dioxide from the role played by sea surface temperatures in changing the TCs characteristics in a warmer world.

The paper is organized as follows. Section 2 describes data, models, simulations and provides an overview of the methodology used. Section 3 presents the results of the analyses, while Section 4 summarizes the main points of the study and concludes the paper.

2. Data and Methodology

2.1. *Reference data*

The reference data used in this study are TC tracks and precipitation. For the former, we use TC observational datasets available as 6-hourly data from the National Hurricane Center (NHC) and the U.S. Joint Typhoon Warning Center (JTWC). These datasets include the location of the center of circulation, maximum wind and minimum pressure for all the TCs during the period 1997-2006. Over the same period, the Global Precipitation Climatology Project (GPCP; Huffman et al. 2001; Bolvin et al., 2009) represents the reference data to quantify the amount of water associated with TCs. GPCP data set is obtained by combining satellite and rain gage data to provide daily global rainfall estimates with a one degree resolution.

2.2. *The climate models*

To investigate the ability of GCMs in representing TCP and its possible changes in a warmer climate, we leverage on a set of simulations performed within the US-CLIVAR Hurricane Working Group. Here we focus on two models, one run by the Geophysical Fluid Dynamics Laboratory (GFDL) and one by the Centro Euro-Mediterrraneo sui Cambiamenti Climatici (CMCC). The GFDL model is a newer version of the High Resolution Atmospheric Model (HIRAM) utilized in Zhao et al. (2009, 2010), and Held and Zhao (2011) for studies of global hurricane climatology, variability, and change with global warming. The main difference is that the HIRAM2.2 incorporates a new land model (GFDL LM3). The atmospheric dynamical core of the model was also updated to improve efficiency and stability. As a result of these changes, there are minor retunings of the atmospheric parameters in the cloud and surface boundary layer parameterizations necessary to achieve the top-of-atmosphere (TOA) radiative balance. This model is also the version of HIRAM used for the GFDL participation in the Fifth Assessment Report of the Intergovernmental Panel on Climate Change (IPCC AR5) high-resolution time-slice simulations. The model uses a finite-volume dynamical core with a cubed-sphere grid topology (Putman and Lin, 2007) and 32 vertical levels. The notation C180 in the model name indicates 180 × 180 grid points in each face of the cube; the size of the model grid varies from 43.5 to 61.6 km. The model uses a modified version of the University of Washington Shallow Convection Scheme (UWShCu) (Bretherton et al. 2004, Zhao et al. 2009). The choice of a less intrusive convection scheme is motivated by a desire for allowing the large scale resolved-scale convection to do much of the work.

The CMCC model is ECHAM5 (Roeckner et al. 2003) implemented with a T159 horizontal resolution, corresponding to a Gaussian grid of about $0.758^{o} \times 0.758^{o}$ with 31 hybrid sigma-pressure levels with top at 10 hPa. The parameterization of convection is based on the mass flux concept (Tiedtke 1989), modified following Nordeng (1994). Moist processes are treated using a mass conserving algorithm for the transport (Lin and Rood 1996) of the different water species and potential chemical tracers. The transport is resolved on the Gaussian grid. A more detailed

description of the ECHAM5 atmospheric model performance can be found in Roeckner et al. (2006).

Rather than running the same TC tracking algorithm on both the GFDL and CMCC models, we used the tracks provided by each modelling group (Shaevitz et al. 2013). The TC tracking algorithm for the CMCC model is based on Walsh (1997) and Walsh et al. (2007) and the tracking for the GFDL model is based on Zhao et al. (2009) and Knutson et al. (2007). Detailed information on the ability of climate models in representing TCs can be found in Walsh et al. (2013).

2.3. *The simulations*

In this study we consider a subset of the simulations available from the US-CLIVAR Hurricane Working Group data set. More specifically, we use the following four experiments:

CLIM: this is a climatological run obtained by repeating the SST climatology over the period 1982-2005 (based on the Hadley Centre Sea Ice and Sea Surface Temperature data set - HadISST, Rayner et al. 2003) for ten years. It is used to provide a baseline to contrast with the perturbation studies. Ozone and aerosols forcings are climatological as provided within the Intergovernmental Panel on Climate Change (IPCC). Also radiative gases concentrations are defined according to the 1992 IPCC specifications and described at the web page http://data1.gfdl.noaa.gov/nomads/forms/TropicalCyclones/exper1.html.

2C: this is a doubling CO_2 experiment. It is obtained by integrating the models with climatological SST (as in CLIM) but with a doubled concentration of atmospheric CO_2 with respect to the CLIM experiment for ten years.

2K: this experiment is obtained by integrating the models with climatological SST (as in CLIM) and adding a 2 K globally-uniform SST anomaly for ten years.

2C2K: This experiment is made by combining the 2K and 2C perturbations.

136

137

138 *2.4. Methodology*

139 The amount of rainfall associated with a TC, both in models and observations, is computed by
140 considering the daily precipitation in a $10^{o}\times10^{o}$ box around the center of the storm. According to
141 previous studies (e.g. Lonfat et al. 2004, Larson et al. 2005, Kunkel et al. 2010) a $10^{o}\times10^{o}$ window
142 (here defined as Box1100) is more than enough to include the majority of TC related precipitation
143 in most of the cases. Moreover, to better represent the contribution of the most intense precipitation
144 patterns close to the TC eye (Villarini et al. 2013), we run the analysis also considering a smaller
145 window ($6^{o}\times6^{o}$, here defined as Box660).

146 # 3. Results

147 *3.1. Present day performance*

148 The control simulation (CLIM) performed with the two models reproduces reasonably well the
149 TC count at the global scale for the present climate, with a 9% underestimation for the CMCC
150 model and a 16% overestimation for the GFDL model, compared to the reference value of 93.3
151 TCs/year obtained from the observation for the period 1997-2006 (Table 1). The CMCC model also
152 tends to significantly underestimate the TC count in the Atlantic basin (not shown) as confirmed by
153 similar analyses using the coupled version of the ECHAM5 atmospheric model (Scoccimarro et al.
154 2011). The simulated interannual variability is slightly overestimated by both models (Table 1).

155 In terms of annual precipitation, both models show a positive bias over the tropical belt (not
156 shown), especially over the intertropical convergence zone (ITCZ) and the South Pacific
157 convergence zone (SPCZ). The difficulty in reproducing the observed precipitation patterns over
158 these areas is a well-known problem common to many atmospheric models and is likely related to a

still unsatisfactory representation of convection and planetary boundary layer processes (Dai, 2006), though remote processes may also contribute (*e.g.*, Hwang and Frierson 2013).

In this work, we aim to assess the models' ability in simulating precipitation associated with TCs, and quantifying their relative changes for the three different idealized global forcing scenarios. To examine the TCP contribution to total precipitation, we accumulated TCP over the 10-year period - representing the present climate and we compared it to the total precipitation for the same period. Figures 1 and 2 show the results for the observations (upper panel) and models (middle and bottom panels), using Box660 and Box1100 windows, respectively. In the observations the TC rainfall represents a large contribution to the total rainfall over the North West Pacific, North East Pacific, and North Western part of the Australian basin. Over these regions, the amount of precipitation contribution due to TCs is as large as about 40%, reaching a maximum of 50% in the North West Pacific. These features are captured by the simulations, despite the tendency of the CMCC model to underestimate the TCP fraction, which is presumably due, at least in part, to the ECHAM5 model deficiency in representing TCs intensity at the global scale and to the lack of TC activity over the Atlantic region (Scoccimarro et al., 2011). Noteworthy, increasing the dimension of the accumulating window (Box1100 in Figure 2 compared to Box660 in Figure 1), the amount of TCP fraction increases especially over the regions with high TC rainfall contributions, suggesting that resorting to a $10^{o} \times 10^{o}$ box does not lead to the inclusion of non-TC related rainfall; rather it seems to provide a representation of TCP fraction consistent with Kunkel et al. (2010). Noteworthy, the CMCC model exhibits an excess of TCP in the Bay of Bengal, which might at least in part explain the positive model bias in the mean precipitation over this region (not shown). In terms of absolute values, the modelled TCP zonal average, normalized by TC days (hereafter TCPn) shows maximum values at about 15^{o} in both hemispheres (Figure 3). Both CMCC and GFDL models are able to represent the basic aspects of the latitudinal distribution of TCPn, with the GFDL model showing a better agreement to the observations, in particular in the Box1100 case (Figure 3, right panel). Also, focusing on coastal regions (Figure 4), the Box1100 TCPn tends to follow more

185 closely the observational results compared to Box660 (Figure 5). In the Box1100 case, the model
186 biases are less pronounced, with a positive value of about 6 mm/day south of 25^{o}S in both models
187 and a meridional variability more (less) pronounced for the CMCC (GFDL) model.

188 *3.2. Impact of idealized forcing*

189 In this section we show the results obtained in the 2C, 2K and 2C2K experiments and contrast
190 them to the control simulation (CLIM). Even though the CLIM results using the Box1100 window
191 seems to more closely reproduce the total precipitation associated with TCs in the observations, we
192 computed changes in TCPn using both windows (Box660 and Box1100, left and right panels
193 respectively in Figures 6 and 7). Performing the analyses on both boxes allows the assessment of
194 the changes associated with the most intense precipitation occurring close to the TC eye (i.e. the
195 results obtained with the Box660 window).

196 Changes in TCPn are very similar for the two models, and show a global increase in the 2K and
197 2C2K experiments but not for the 2C one. The meridional distribution of TCPn changes (Figure 6)
198 in the 2C case shows negative values over most of the latitudes. On the other hand, the 2K and
199 2C2K experiments show positive changes up to 45% when considering the average of the two
200 models (figure 6, red and green bold lines). The positive increase is more pronounced in the 2K
201 experiment if compared to the 2C2K one. These results are consistent with Villarini et al. (2013)
202 who found a widespread decrease in rainfall for the most intense TCs for the 2C experiment and a
203 general increase in rainfall when SST was increased by 2K. This statement holds regardless of the
204 distance from the center of circulation and for all the ocean basins.

205 Focusing on the coastal region (shaded area in figure 4), the TCPn increase in 2K and 2C2K is
206 even more pronounced (Figure 7), up to 200%. In these areas even the 2C experiment shows
207 positive changes in most latitudes. Interestingly the TCPn increase over the coastal regions (Figure
208 7) is less marked at latitudes already exposed to large amount of TCPn (i.e., between 10^{o}-15^{o} in the
209 northern hemisphere and 10^{o}-20^{o} in the southern hemisphere; see Figure 5) and more evident

northward and equatorward these belts, leading to a more uniform distribution of TCPn with latitude in a warmer climate.

4. Discussion and Conclusions

It is well known that atmospheric moisture content tends to increase at a rate roughly governed by the Clausius–Clapeyron equation, while the energy available to drive convection (such as the ability of the troposphere to radiate away latent heat) increases more slowly (e.g., Knutson and Manabe 1995; Allen and Ingram 2002; Held and Soden 2006; Meehl et al. 2007). Therefore in a warmer climate we expect an increase in the water amount associated with phenomena leading to intense precipitation (such as TCs) larger than what it is expected in moderate events (Scoccimarro et al., 2013). Other studies (e.g., Hill and Lackmann 2009, Wu et al. 2012) suggest that larger environmental relative humidity lead to the establishment of wider TCs (associated with larger storms), thus more available precipitable water. In addition Matyas and Cartaya (2009) determined that the TC precipitation distribution is influenced by the degree of outer rainband activity, which, in turn, is related to environmental specific humidity.

Our results show that the TCP is increased in the experiments with a 2K-SST increase. On the other hand, in the simulation with doubling of atmospheric CO_2, the changes in TC rainfall are small and we found that, on average, the simulated TC rainfall tends to decrease compared to the present day climate (Figure 6). Since environmental humidity was found to correlate with a larger hurricane rain field (Matyas, 2010), and because we should expect a strong relationship between changes in available precipitable water and changes in TCP, we investigated changes in the vertically integrated atmospheric water content (WCONT) under the different idealized warming scenarios (Figure 8). All the considered experiments show an increase in the water content over the tropical belt. The percentage increase is almost uniform across latitudes (Figure 8, right panel and Table 2), leading to a more pronounced absolute increase over the warmer (equatorial) regions, where the WCONT shows its maxima in the CLIM experiment (not shown). The WCONT

235 percentage increase is about 1% in 2C (statistically significant at the 95% level according to a t-test,
236 over most of the latitudes, especially in the northern hemisphere, not shown), 18% in 2K and 19%
237 in 2C2K, suggesting that the 1% increment between 2K and 2C2K is mainly due to the higher
238 atmospheric capability to hold moisture induced by the doubling of CO_2, as shown in the 2C
239 experiment: in this experiment the globally averaged surface temperature increases of about 0.1K,
240 due to the warming over land. The described WCONT increases follow the Clausius–Clapeyron
241 relation (CC) since climate models obey CC scaling fairly closely (Held and Soden, 2006).
242 According to the CC, the lower-tropospheric temperature change found in the different experiments
243 (about 0.1 K in the 2C, 2.2 K in the 2K and 2.4 K in the 2C2K) should leads to a WCONT increase
244 of about 1%, 18% and 19% respectively, which is fully consistent with what is obtained from the
245 models.

246 Despite the increase in WCONT in all of the three warming experiments, the doubling of CO_2
247 tends to reduce TCP, whereas the increase of 2 K in SST tends to increase TCP. The reason should
248 be found in the water balance at the surface: in 2K and 2C2K experiments (2Ks) we found a strong
249 increase of the evaporation rate over the tropics (Figure 9, green and red lines respectively) due to
250 the increase in saturated water vapour pressure at the surface. The 2K-increase in SST leads to a net
251 increase of the evaporation rate (E). This can be easily explained considering that E is proportional
252 to the difference between saturated water vapour at the surface (e_s) and water vapour pressure of the
253 lower tropospheric layers (e_a), and that e_s depends on surface temperature following an exponential
254 law, whereas e_a follows the same law, scaled by a factor (less than 1) represented by the relative
255 humidity. Therefore an increase in temperature has different impacts on e_s and e_a. The doubling of
256 CO_2, on the other hand, tends to reduce E (Figure 9, blue line: the reduction is small but statistically
257 significant at the 95% level according to a t-test, over most of the tropical domain, not shown)
258 independently of the boundary conditions. The doubling of CO_2 in forced experiments (prescribed
259 SST) induces a weakening effect on E, since the increase in the lower tropospheric temperature
260 leads to an increase in e_a, associated with no changes in e_s due to the fixed temperature forcing at

261 the surface. This effect results in an increase of the atmospheric static stability in the 2C
262 experiment.

263 The CO_2 doubling tends to slow down the global hydrological cycle by about 2% (see Table 2).
264 This is also evident in the meridional distribution of evaporation and precipitation changes (blue
265 lines in Figure 9 and 10, respectively) during the TC season. The 2 K SST increase induces an
266 acceleration of the hydrological cycle of the order of 6-7% that is reduced to 4-5% if associated
267 with the CO_2 doubling (Table 2, Figures 9 and 10). The changes found in the hydrological cycle are
268 strongly influenced by the TC precipitation: a 4% / 6% (2C2K / 2K) increase in the average
269 precipitation corresponds to an increase of about 20% / 30% in TC related precipitation.

270 In summary, the precipitation associated with TCs results in an increase in the experiments with
271 a 2 K-SST increase and to a decrease when atmospheric CO_2 is doubled. This is consistent with the
272 water balance at the surface, as a 2 K-increase in SST leads to a net increase of the evaporation
273 rate, while doubling the atmospheric CO_2 has the opposite effect. Moreover TCPn (Figure3) tends
274 to increase in a warmer climate (Figure 6) leading to a more uniform latitudinal distribution of the
275 projected precipitation associated with TCs. This is confirmed over land (Figures 5 and 7) where
276 the TCPn increase is projected in all of the considered warming scenarios.

277

278 ***Acknowledgments***. This work was carried out as part of a Hurricane and Climate Working Group
279 activity supported by the U.S. CLIVAR. We acknowledge the support provided by Naomi
280 Henderson, who downloaded and organized the data at the Lamont data library. The research
281 leading to these results has received funding from the Italian Ministry of Education, University and
282 Research and the Italian Ministry of Environment, Land and Sea under the GEMINA project.
283 Moreover this material is based in part upon work supported by the National Science Foundation
284 under Grant No. AGS-1262099 (Gabriele Villarini and Gabriel A. Vecchi).

285

References

Allen, M. R., and W. J. Gram, 2002: Constraints on future changes in climate and the hydrologic cycle. *Nature*, 419, 224–232.

Anderson, J., and Coauthors, 2004: The new GFDL global atmosphere and land model AM2/LM2: Evaluation with prescribed SST simulations. *J. Climate*, 17, 4641–4673.

Bolvin, D. T., R. F. Adler, G. J. Huffman, E. J. Nelkin, and J. P. Poutiainen, 2009: Comparison of GPCP monthly and daily precipitation estimates with high-latitude gauge observations. *J. Appl. Meteor. Climatol.*, 48, 1843–1857.

Bretherton, C. S., J. R. McCaa, and H. Grenier, 2004: A new parameterization for shallow cumulus convection and its application to marine subtropical cloud-topped boundary layers. Part I: Description and 1D results. *Mon. Wea. Rev.*, 132, 864–882.

Chou, C., J. D. Neelin, C. Chen, and J. Tu, 2009: Evaluating the 'rich-get-richer' mechanism in tropical precipitation change under global warming. *J. Climate*, 22, 1982–2005.

Corbosiero, K.L., M.J. Dickinson, L.F. Bosart, 2009: The Contribution of Eastern North Pacific Tropical Cyclones to the Rainfall Climatology of the Southwest United States. *Mon. Wea. Rev.*, 137, 2415–2435.doi: http://dx.doi.org/10.1175/2009MWR2768.1

Dai, Aiguo, 2006: Precipitation Characteristics in Eighteen Coupled Climate Models. *J. Climate*, 19, 4605–4630.

Dare, Richard A., Noel E. Davidson, John L. McBride, 2012: Tropical Cyclone Contribution to Rainfall over Australia. *Mon. Weather Rev.*, 140, 3606–3619. doi: http://dx.doi.org/10.1175/MWR-D-11-00340.1

Gualdi, S., E. Scoccimarro, A. Navarra, 2008: Changes in tropical cyclone activity due to global warming: Results from a high-resolution coupled general circulation model. *J. Climate*, 21, 5204–5228.

Hasegawa A, S. Emori, 2005: Tropical cyclones and associated precipitation over the western North Pacific in present and doubled CO_2 climates simulated by a T106 atmospheric GCM. *SOLA*, 1,145-148.

Held, I. M. and B.J. Soden, 2006: Robust responses of the hydrological cycle to global warming. *J. Climate* 19, 5686–5699.

Held, I. M., and M. Zhao, 2011: The response of tropical cyclone statistics to an increase in CO2 with fixed sea surface temperatures. *J. Climate*, 24(20), DOI:10.1175/JCLI-D-11-00050.1.

Hill, K. A., and G. M. Lackmann, 2009: Influence of environmental humidity on tropical cyclone size. *Mon. Weather Rev.*, 137, 3294–3315, doi:10.1175/2009MWR2679.1.

Huffman, G.J., R.F. Adler, M. Morrissey, D.T. Bolvin, S. Curtis, R. Joyce, B. McGavock, and J. Susskind, 2001: Global precipitation at onedegree daily resolution from multi-satellite observation. *J. Hydrometeorol.*, 2, 36–50.

Hwang, Y.-T., and D.W.M. Frierson, 2013: Link between the double-Intertropical Convergence Zone problem and cloud biases over the Southern Ocean. *Proc. Nat. Acad. Sci.*, doi: 10.1073/pnas.1213302110

Jiang, H., E. J. Zipser, 2010: Contribution of Tropical Cyclones to the Global Precipitation from Eight Seasons of TRMM Data: Regional, Seasonal, and Interannual Variations. *J. Climate*, 23, 1526–1543.

Knutson, T. R., and S. Manabe, 1995: Time-mean response over the tropical Pacific to increased CO2 in a coupled ocean– atmosphere model. *J. Climate*, **8**, 2181–2199.

Knutson, T. R., and R. E. Tuleya, 2004: Impact of CO2-induced warming on simulated hurricane intensity and precipitation: Sensitivity to the choice of climate model and convective parameterization. *J. Climate*, 17(18), 3477-3495.

Knutson, T. R., J. J. Sirutis, S. T. Garner, I. M. Held, R. E. Tuleya, 2007: Simulation of the Recent Multidecadal Increase of Atlantic Hurricane Activity Using an 18-km-Grid Regional Model. *Bull. Amer. Meteor. Soc*., 88, 1549–1565. doi: http://dx.doi.org/10.1175/BAMS-88-10-1549

Knutson, T. R., J. McBride, J. Chan, K. A. Emanuel, G. Holland, C. Landsea, I. M. Held, J. Kossin, A. K. Srivastava, and M. Sugi, 2010: Tropical cyclones and climate change. *Nat. Geosci*., 3, 157-163, doi:doi:10.1038/ngeo779.

Knutson, T. R., Sirutis, J. J., Vecchi, G. A., Garner, S., Zhao, M., Kim, H-S., Bender, M., Tuleya, R. E., Held, I. M. and G. Villarini, 2013: Dynamical Downscaling Projections of Twenty-First-Century Atlantic Hurricane Activity: CMIP3 and CMIP5 Model-Based Scenarios. *J. Climate*, 26:17, 6591-6617

Kunkel, K. E., D. Easterling, D. A. R. Kristovich, B. Gleason, L. Stoecker, and R. Smith, 2010: Recent increases in U.S. heavy precipitation associated with tropical cyclones. *Geophys. Res. Lett.*, 37, L24706.

Larson, J., Y. Zhou, R. W. Higgins, 2005: Characteristics of Landfalling Tropical Cyclones in the United States and Mexico: Climatology and Interannual Variability. *J. Climate*, 18, 1247–1262. doi: http://dx.doi.org/10.1175/JCLI3317.1

Lin, S. J., and R. B. Rood, 1996: Multidimensional flux form semi-Lagrangian transport. *Mon. Weather Rev*., 124, 2046–2068.

Liu, S. C., C. Fu, C.-J. Shiu, J.-P. Chen, and F. Wu, 2009: Temperature dependence of global precipitation extremes. *Geophys. Res. Lett.*, 36, L17702, doi:10.1029/ 2009GL040218.

Lonfat, M., Frank D. Marks, Shuyi S. Chen, 2004: Precipitation Distribution in Tropical Cyclones Using the Tropical Rainfall Measuring Mission (TRMM) Microwave Imager: A Global Perspective. *Mon. Weather Rev.*, 132, 1645–1660.

Matyas, C. J., and M. Cartaya, 2009: Comparing the rainfall pat- terns produced by Hurricanes Frances (2004) and Jeanne (2004) over Florida. *Southeastern Geogr.*, 49, 132–156.

Matyas, C.J., 2010: Associations between the size of hurricane rain fields at landfall and their surrounding environments, *Meteorol. Atmos. Phys.*, 106, 3-4, pp 135-148.

Meehl, G. A. and Coauthors, 2007: Global climate projections. Climate Change 2007: The Physical Science Basis, S. Solomon et al., Eds., Cambridge University Press, 747–845.

Mendelsohn, R., K. Emanuel, S. Chonabayashi, and L. Bakkensen, 2012: The impact of climate change on global tropical cyclone damage. *Nat. Clim. Change*, 2, 205-209.

Nordeng, T. E., 1994: Extended versions of the convective parameterization scheme at ECMWF and their impact on the mean and transient activity of the model in the tropics. ECMWF Research Department Tech. Memo. 206, 41 pp.

Peduzzi, P., B. Chatenou, H. Dao, A. De Bono, C. Herold, J. Kossin, F. Mouton, and O. Nordbeck, 2012: Global trends in tropical cyclone risk. *Nat. Climate Change*, 2, 289–294.

Pielke, R.A., J. Gratz, C.W. Landsea, D. Collins, M.A. Saunders, and R. Musulin, 2008: Normalized hurricane damage in the United States: 1900-2005. *Nat. Hazards Rev.*, 9(1), 29–42.

Putman, W.M., and S.-J. Lin, 2007: Finite-volume transport on various cubed-sphere grids. *J. Comput. Phys*., 227, 55–78.

Rayner, N. A. and co-authors, 2003: Global analyses of sea surface temperature, sea ice, and night marine air temperature since the late nineteenth century. *J. Geophys. Res*. 108, D14, 4407 10.1029/2002JD002670

Rappaport, E. N., 2000: Loss of life in the United States associated with recent tropical cyclones. *Bull. Amer. Meteor. Soc.*, 81, 2065–2074.

Roeckner, E., and Coauthors, 2003: The atmospheric general circulation model ECHAM5. Part I: Model description. MPI Rep. 349, 127 pp.

Roeckner E. and Coauthors, 2006: Sensitivity of simulated climate to horizontal and vertical resolution in the ECHAM5 atmosphere model. *J. Climate*, 19, 3771–3791.

Scoccimarro, E., S. Gualdi, A. Bellucci, A. Sanna, P. G. Fogli, E. Manzini, M. Vichi, P. Oddo, and A. Navarra, 2011: Effects of tropical cyclones on ocean heat transport in a high resolution coupled general circulation model. *J. Climate*, 24, 4368–4384, doi:10.1175/2011JCLI4104.1.

Scoccimarro E., S. Gualdi, A. Bellucci, M. Zampieri, A. Navarra, 2013: Heavy precipitation events in a warmer climate: results from CMIP5 models. *J. Climate*, DOI: 10.1175/JCLI-D-12-00850.1.

Shaevitz D. et al., 2013: Characteristics of tropical cyclones in high-resolution models of the present climate. Submitted to *J. Climate.*

Tiedtke, M., 1989: A comprehensive mass flux scheme for cumulus parametrization in large-scale models. *Mon. Wea. Rev*., 117, 1779–1800.

Trenberth, K. E., 2011: Changes in precipitation with climate change. *Climate Research*, 47, 122-138, doi: 10.3354/cr00953.

435 Villarini G., D.A. Lavers, E. Scoccimarro, M. Zhao, M.F. Wehner, G.A. Vecchi, T.R. Knutson, and
436 K. Reed, 2013: Sensitivity of tropical cyclone rainfall to idealized global scale forcings. *J. Climate*
437 in press.
438
439 Walsh, K. J. E., 1997: Objective detection of tropical cyclones in high-resolution analyses. *Mon.*
440 *Weather Rev.*, 125, 958–977.
441
442 Walsh, K. J. E., M. Fiorino, C. W. Landsea, and K. L. McInnes, 2007: Objectively determined
443 resolution-dependent threshold criteria for the detection of tropical cyclones in climate models and
444 reanalyses. *J. Climate*, 20, 2307–2314.
445
446 Walsh, K. J. E., S. Lavender, E. Scoccimarro and H. Murakami, 2013: Resolution dependence of
447 tropical cyclone formation in CMIP3 and finer resolution models. *Clim. Dynam.*, 40, 585–599, doi:
448 10.1007/s00382-012-1298-z.
449
450 Wu, L., H. Su, R. G. Fovell, B. Wang, J. T. Shen, B. H. Kahn, S. M. Hristova-Veleva, B. H.
451 Lambrigtsen, E. J. Fetzer, and J. H. Jiang, 2012: Relationship of environmental relative humidity
452 with North Atlantic tropical cyclone intensity and intensification rate, *Geophys. Res. Lett*., 39,
453 L20809, doi:10.1029/2012GL053546.
454
455 Zhao, M., I. M. Held, S.-J. Lin, and G. A. Vecchi, 2009: Simulations of global hurricane cli-
456 matology, interannual variability, and response to global warming using a 50km resolution GCM. *J.*
457 *Climate*, 22, 6653–6678.

458 Zhao, M., I.M. Held, and G. Vecchi, 2010: Retrospective forecasts of the hurricane season using a
459 global atmospheric model assuming persistence of SST anomalies. *Mon. Wea. Rev.*, 138(10),
460 DOI:10.1175/2010MWR3366.1

461
462

463

	CLIM		2C		2K		2C2K	
	MEAN	STD	MEAN	STD	MEAN	STD	MEAN	STD
OBS	93.3	6.5	-	-	-	-	-	-
CMCC	85.3	9.8	76.6	5.4	88.5	10.8	80.4	8.0
GFDL	109.1	8.0	106.0	7.0	95.3	5.1	84.7	9.7

464 Table 1. Tropical Cyclone count: TC annual mean number and standard deviation of the TC annual

465 number.

466

		CLIM value	2C % change	2K % change	2C2K % change
PRECIPITATION	CMCC	2.9 [mm/d]	-2.3	7.3	4.8
	GFDL	3.0 [mm/d]	-2.2	6.7	4.2
EVAPORATION	CMCC	2.9 [mm/d]	-2.3	7.2	4.7
	GFDL	3.0 [mm/d]	-2.2	6.7	4.2
ATM. WATER CONTENT	CMCC	26.1 [Kg/m^2]	1.3	18.6	20.1
	GFDL	24.1 [Kg/m^2]	1.0	18.2	19.0

467

468 Table 2. Water balance at the global scale.

469

Figure captions:

FIG. 1. Percentage of water associated with TCs in the control simulation CLIM with respect to the total annual precipitation. The accumulation is performed by taking a $6^o \times 6^o$ window centered on the center of circulation. The upper panel refers to the observations, while the central and lower panels to the CMCC and GFDL models, respectively. Units are [%].

FIG. 2. Same as Figure 1 but performing the accumulation for a $10^o \times 10^o$ window.

Fig.3. TC related precipitation amount in the CLIM experiment and observations as a function of latitude at global scale. Values are normalized by the number of TC days. Units are [mm/d].

Fig.4. Coastal regions mask. Precipitation over land is accumulated considering the gray region only.

Fig.5. TC related precipitation amount in the CLIM experiment and observations as a function of latitude computed over considered land regions as defined in Figure 4. Values are normalized by the number of TC days. Units are [mm/day].

Fig.6. Changes in TC related precipitation amount in the 2C (blue), 2K (green) and 2C2K (red) experiments as a function of latitude. Results are shown with respect to the CLIM experiment. Solid thin lines represent CMCC results. Dashed thin lines represent GFDL results. The solid thick lines represent the average of the two models. Units are [%].

Fig.7. Same as Figure 6 but for the land regions defined in Figure 4.

Fig.8. Changes in vertically integrated water content (WCONT) in 2C (blue), 2K (green) and 2C2K (red) experiments as a function of latitude with respect to the CLIM experiment. Solid thin lines represent CMCC results. Dashed thin lines represent GFDL results. Solid thick lines represent averaged values. Northern hemisphere values are computed over JJASON and Southern Hemisphere values are computed over DJFMAM. Units are [kg/m^2] (left panel) and [%] (right panel).

Fig.9. Changes in evaporation (EVAP) in 2C (blue), 2K (green) and 2C2K (red) experiments as a function of latitude with respect to the CLIM experiment. Solid thin lines represent CMCC results. Dashed thin lines represent GFDL results. Solid thick lines represent averaged values. Northern hemisphere values are computed over JJASON and Southern Hemisphere values are computed over DJFMAM. Units are [mm/d] (left panel) and [%] (right panel).

Fig.10. Changes in precipitation (PRECIP) in 2C (blue), 2K (green) and 2C2K (red) experiments as a function of latitude with respect to the CLIM experiment. Solid thin lines represent CMCC results. Dashed thin lines represent GFDL results. Solid thick lines represent averaged values. Northern hemisphere values are computed over JJASON and Southern Hemisphere values are computed over DJFMAM. Units are [mm/d] (left panel) and [%] (right panel).

506

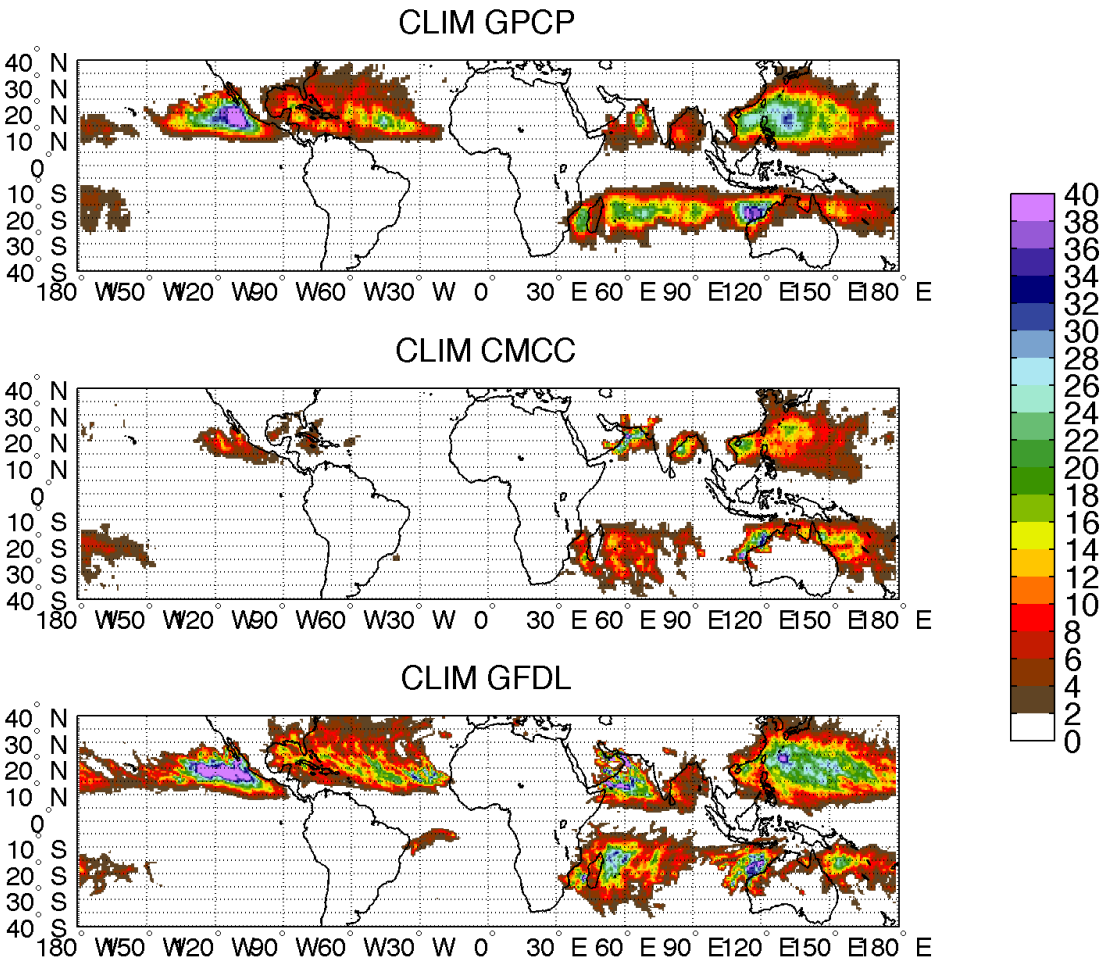

507

508 FIG. 1. Percentage of water associated with TCs in the control simulation CLIM with respect to the
509 total annual precipitation. The accumulation is performed by taking a $6^{o}\times6^{o}$ window centered on the
510 center of circulation. The upper panel refers to the observations, while the central and lower panels
511 to the CMCC and GFDL models, respectively. Units are [%].

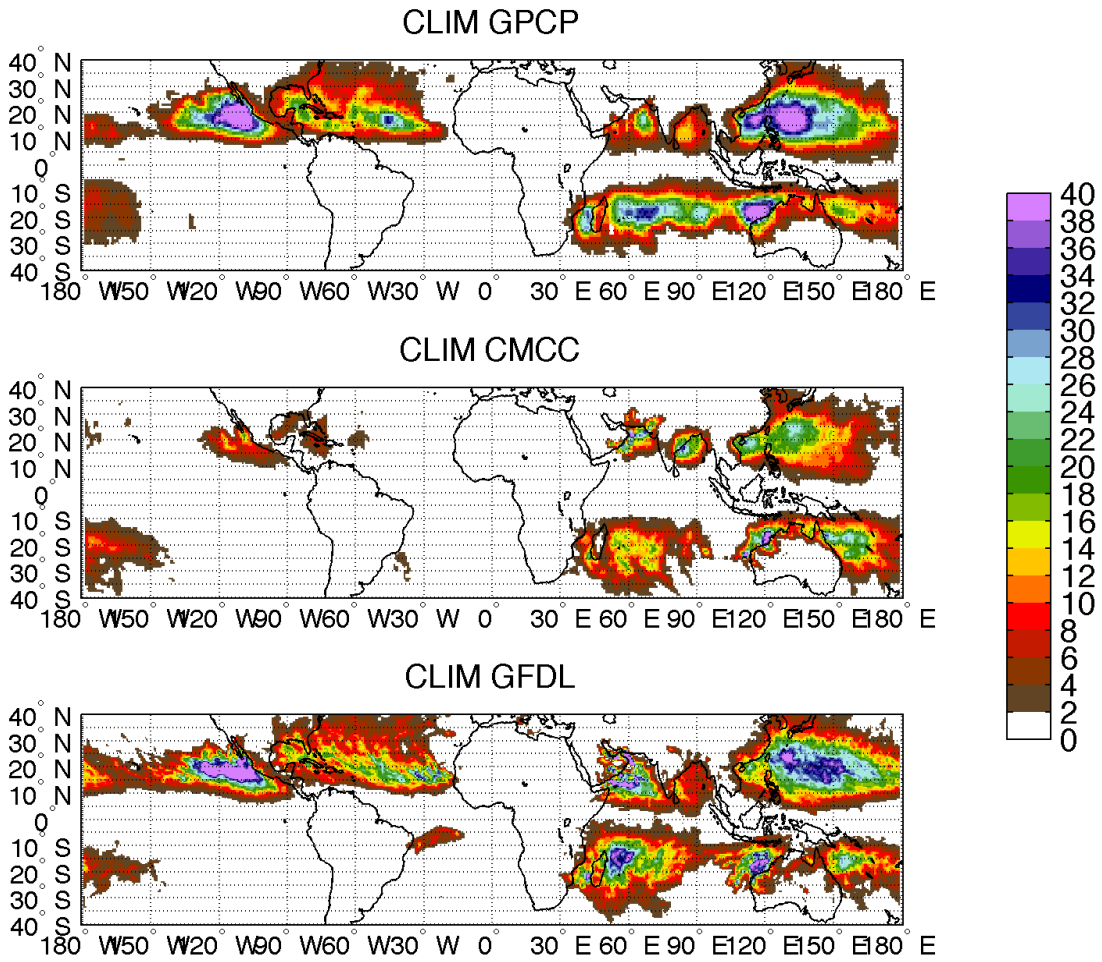

512

513 FIG. 2. Same as Figure 1 but performing the accumulation for a $10^{o}\times10^{o}$ window.

514

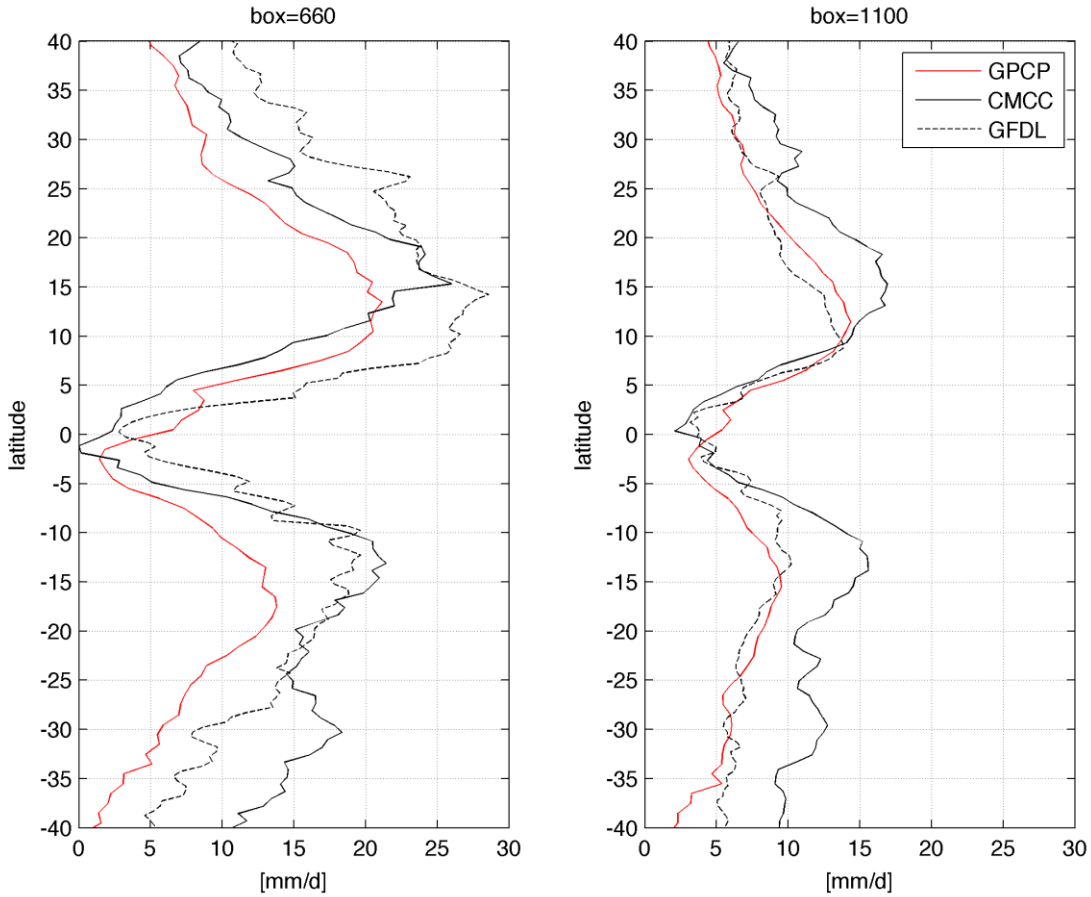

515

516 Fig. 3. TC related precipitation amount in the CLIM experiment and observations as a function of
517 latitude at the global scale. Values are normalized by the number of TC days. Units are [mm/d].

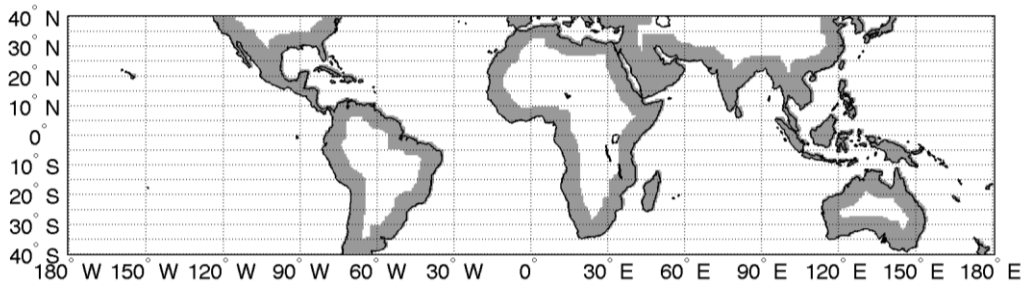

518

519 Fig. 4. Coastal regions mask. Precipitation over land is accumulated considering the gray region
520 only.

521

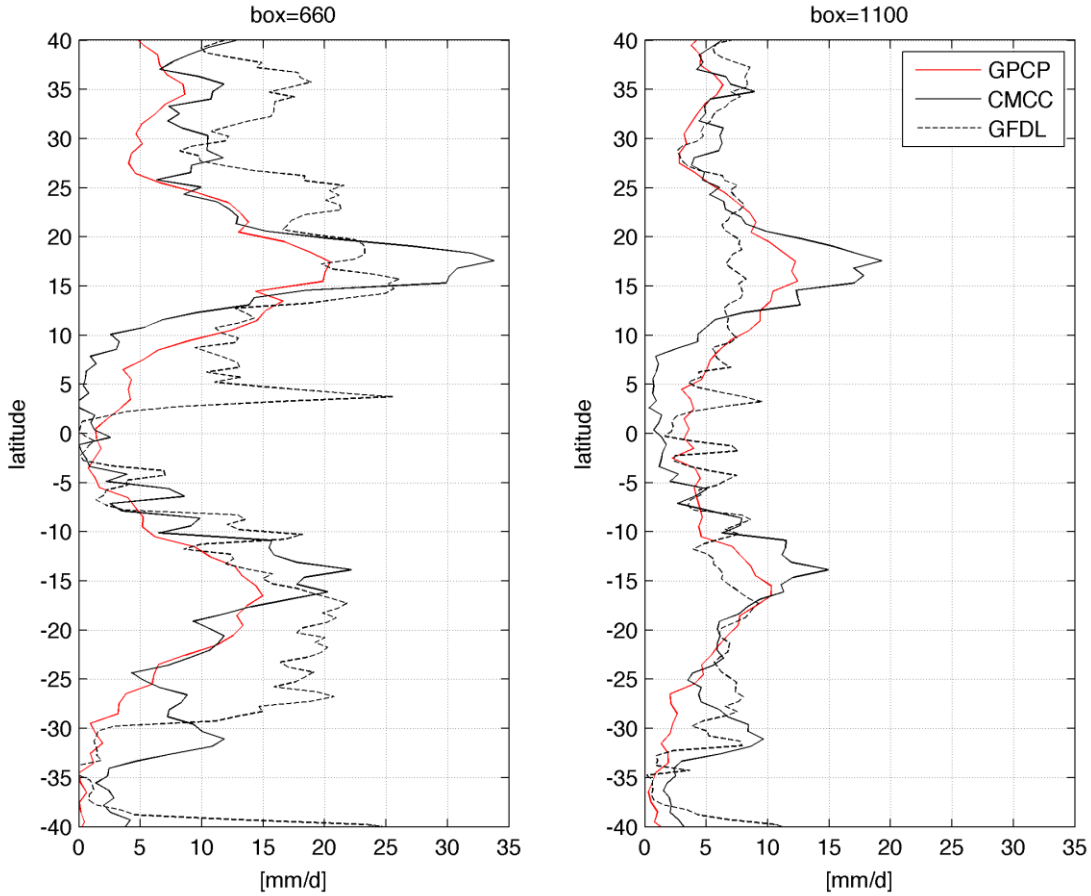

522

523 Fig. 5. TC related precipitation amounts in the CLIM experiment and observations as a function of
524 latitude computed over considered land regions as defined in Figure 4. Values are normalized by
525 the number of TC days. Units are [mm/day].

526

527

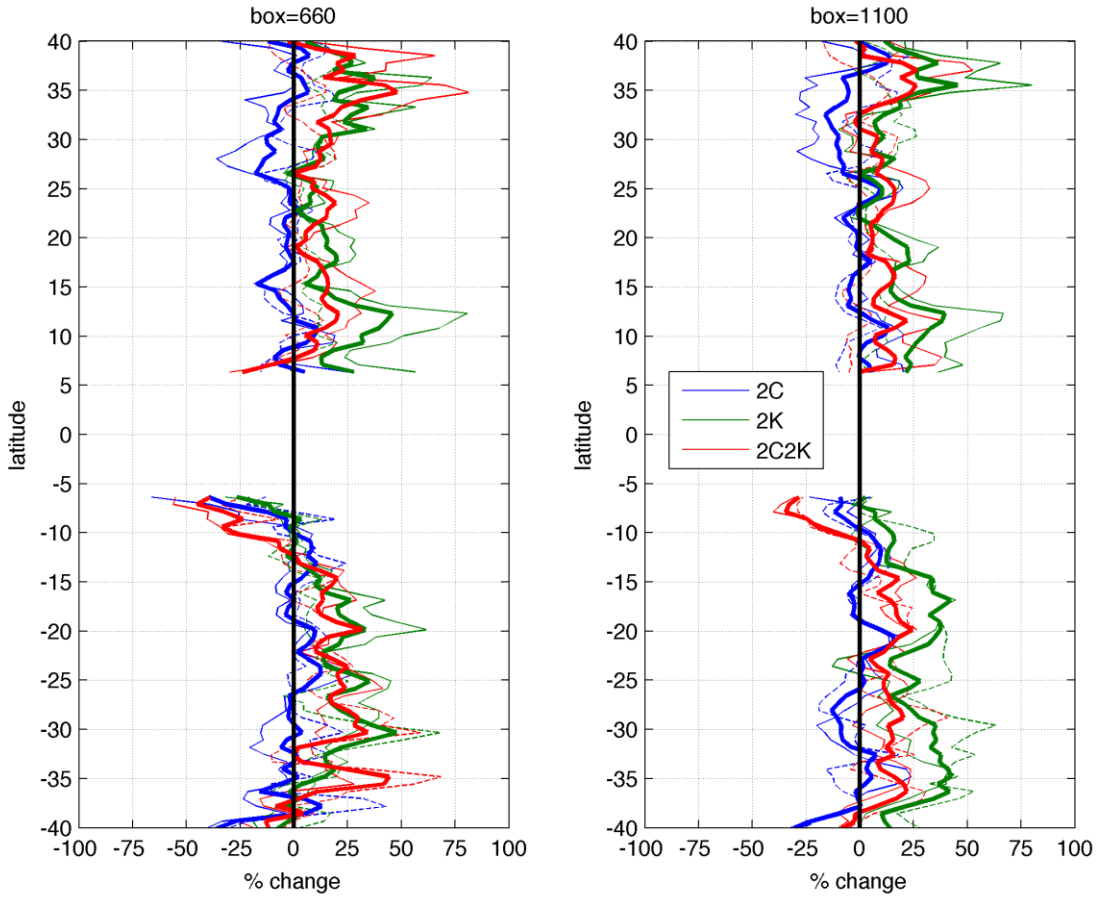

528

529 Fig. 6. Changes in TC related precipitation amount in the 2C (blue), 2K (green) and 2C2K (red)
530 experiments as a function of latitude. Results are shown with respect to the CLIM experiment. Solid
531 thin lines represent CMCC results. Dashed thin lines represent GFDL results. The solid thick lines
532 represent the average of the two models. Units are [%].

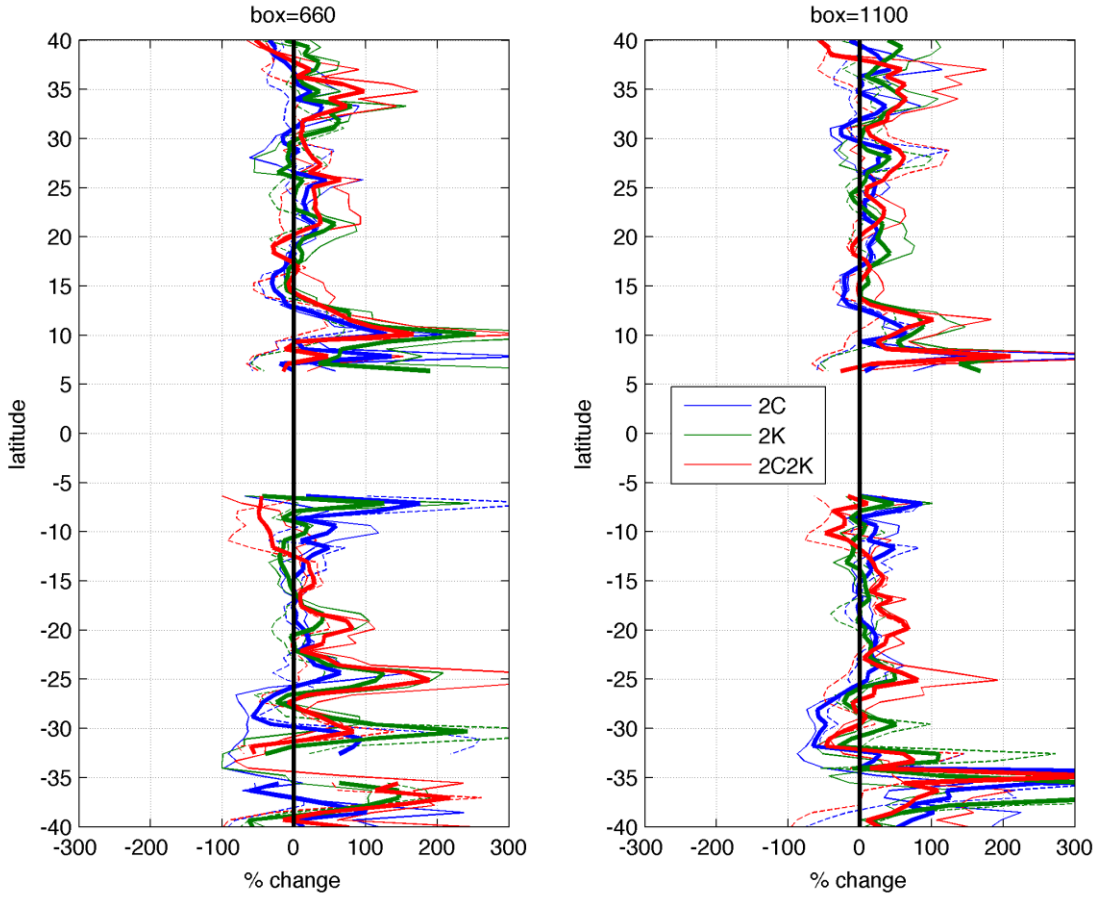

533

534 Fig. 7. Same as Figure 6 but for the land regions defined in Figure 4.

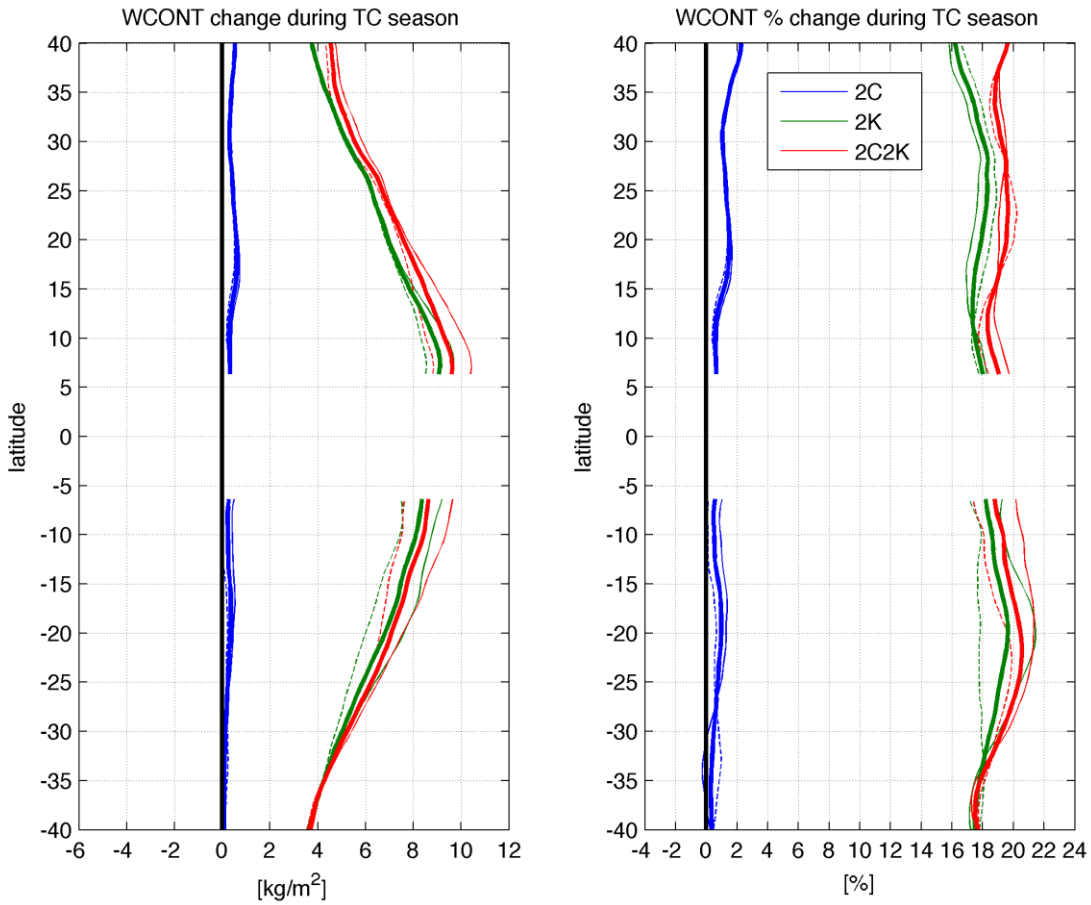

535

536 Fig. 8. Changes in vertically integrated water content (WCONT) in 2C (blue), 2K (green) and 2C2K
537 (red) experiments as a function of latitude with respect to the CLIM experiment. Solid thin lines
538 represent CMCC results. Dashed thin lines represent GFDL results. Solid thick lines represent
539 averaged values. Northern hemisphere values are computed over JJASON and Southern
540 Hemisphere values are computed over DJFMAM. Units are [kg/m^2] (left panel) and [%] (right
541 panel).

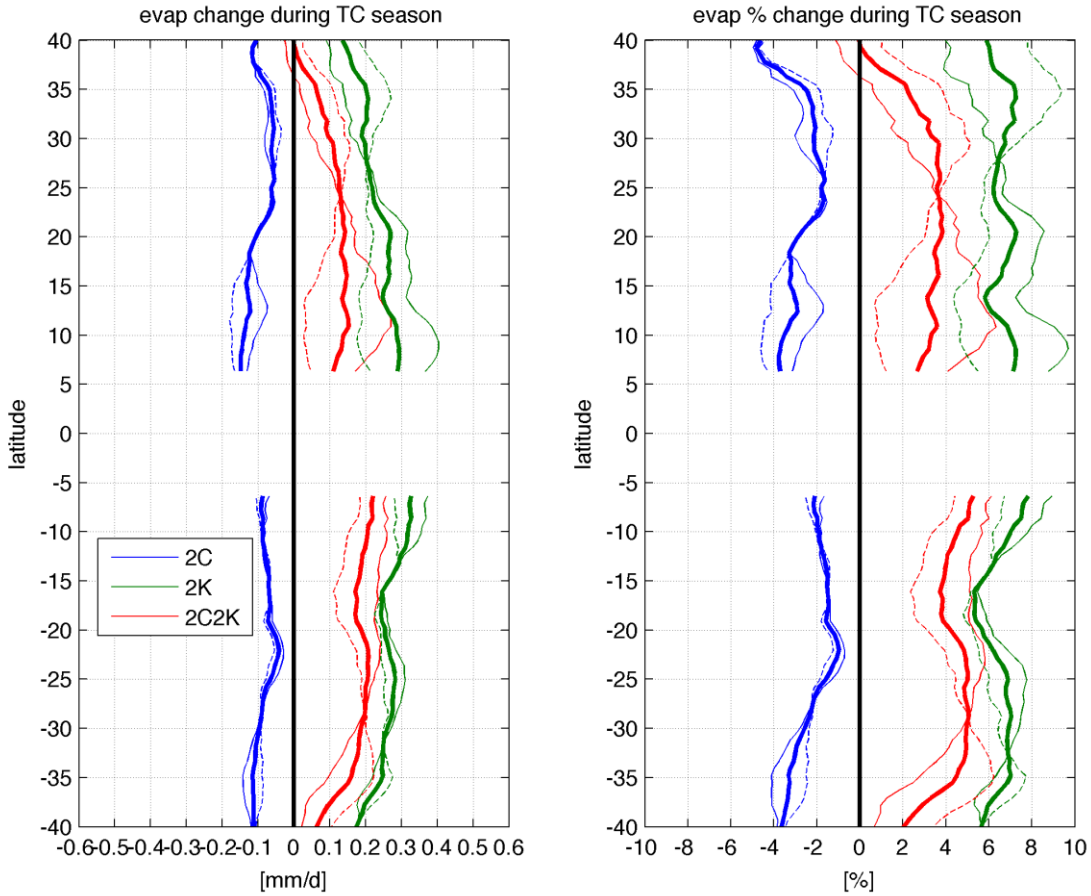

542

543 Fig. 9. Changes in evaporation (EVAP) in 2C (blue), 2K (green) and 2C2K (red) experiments as a
544 function of latitude with respect to the CLIM experiment. Solid thin lines represent CMCC results.
545 Dashed thin lines represent GFDL results. Solid thick lines represent averaged values. Northern
546 hemisphere values are computed over JJASON and Southern Hemisphere values are computed over
547 DJFMAM. Units are [mm/d] (left panel) and [%] (right panel).

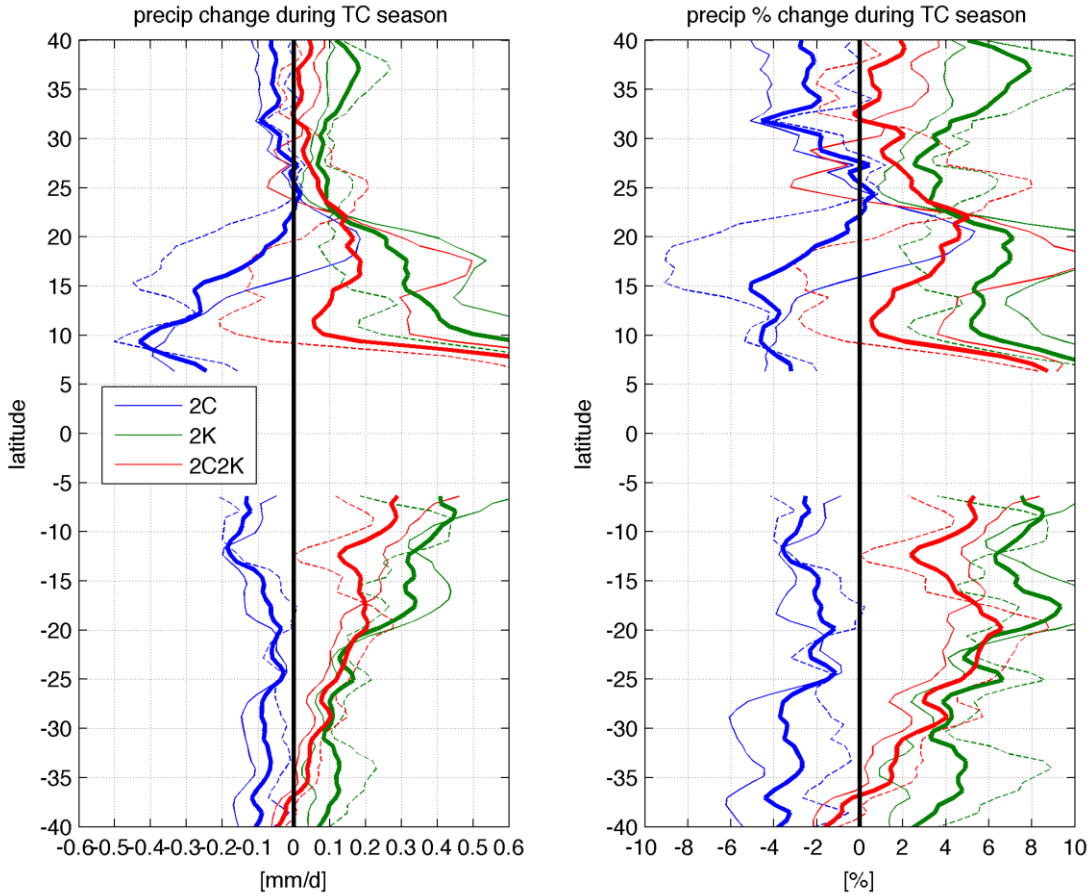

548

549 Fig. 10. Changes in precipitation (PRECIP) in 2C (blue), 2K (green) and 2C2K (red) experiments as
550 a function of latitude with respect to the CLIM experiment. Solid thin lines represent CMCC
551 results. Dashed thin lines represent GFDL results. Solid thick lines represent averaged values.
552 Northern hemisphere values are computed over JJASON and Southern Hemisphere values are
553 computed over DJFMAM. Units are [mm/d] (left panel) and [%] (right panel).

554